electronics

MDPI

Article

Investigation of Future 5G-IoT Millimeter-Wave Network Performance at 38 GHz for Urban Microcell Outdoor Environment

Faizan Qamar [1], MHD Nour Hindia [1], Kaharudin Dimyati [1,*], Kamarul Ariffin Noordin [1], Mohammed Bahjat Majed [2], Tharek Abd Rahman [3] and Iraj Sadegh Amiri [4,5,*]

1 Department of Electrical Engineering, Faculty of Engineering, University of Malaya, Kuala Lumpur 50603, Malaysia; engr.faizanq@gmail.com (F.Q.); nourhindia@hotmail.com (M.N.H.); kamarul@um.edu.my (K.A.N.)
2 Department of Computer Science, College of Science and Technology, University of Human Development (UHD), Sulaymaniyah 00964, KRG, Iraq; mohammed.majed@uhd.edu.iq
3 Wireless Communication Centre, Faculty of Electrical Engineering, Universiti Teknologi Malaysia, Johor 81310, Malaysia; tharek@fke.utm.my
4 Computational Optics Research Group, Advanced Institute of Materials Science, Ton Duc Thang University, Ho Chi Minh City 700000, Vietnam
5 Faculty of Applied Sciences, Ton Duc Thang University, Ho Chi Minh City 700000, Vietnam
* Correspondence: kaharudin@um.edu.my (K.D.); irajsadeghamiri@tdtu.edu.vn (I.S.A.)

Received: 2 April 2019; Accepted: 24 April 2019; Published: 3 May 2019

Abstract: The advent of fifth-generation (5G) systems and their mechanics have introduced an unconventional frequency spectrum of high bandwidth with most falling under the millimeter wave (mmWave) spectrum. The benefit of adopting these bands of the frequency spectrum is two-fold. First, most of these bands appear to be unutilized and they are free, thus suggesting the absence of interference from other technologies. Second, the availability of a larger bandwidth offers higher data rates for all users, as there are higher numbers of users who are connected in a small geographical area, which is also stated as the Internet of Things (IoT). Nevertheless, high-frequency band poses several challenges in terms of coverage area limitations, signal attenuation, path and penetration losses, as well as scattering. Additionally, mmWave signal bands are susceptible to blockage from buildings and other structures, particularly in higher-density urban areas. Identifying the channel performance at a given frequency is indeed necessary to optimize communication efficiency between the transmitter and receiver. Therefore, this paper investigated the potential ability of mmWave path loss models, such as floating intercept (FI) and close-in (CI), based on real measurements gathered from urban microcell outdoor environments at 38 GHz conducted at the Universiti Teknologi Malaysia (UTM), Kuala Lumpur campus. The measurement data were obtained by using a narrow band mmWave channel sounder equipped with a steerable direction horn antenna. It investigated the potential of the network for outdoor scenarios of line-of-sight (LOS) and non-line-of-sight (NLOS) with both schemes of co- (vertical-vertical) and cross (vertical-horizontal) polarization. The parameters were selected to reflect the performance and the variances with other schemes, such as average users cell throughput, throughput of users that are at cell-edges, fairness index, and spectral efficiency. The outcomes were examined for various antenna configurations as well as at different channel bandwidths to prove the enhancement of overall network performance. This work showed that the CI path loss model predicted greater network performance for the LOS condition, and also estimated significant outcomes for the NLOS environment. The outputs proved that the FI path loss model, particularly for V-V antenna polarization, gave system simulation results that were unsuitable for the NLOS scenario.

Keywords: 5G; 38 GHz; millimeter wave; channel propagation; path loss; MIMO

1. Introduction

In a 5G communication network, mobile operators are forced to use a high-frequency spectrum due to the limited amount of channel bandwidth. The 5G boosts the overall performance and enhances user experience offered by the present generation mobile technologies. Some of the most hyped features include higher data-rates, lower end-to-end delays, and minimal energy consumption [1]. In order to meet a common goal, several technologies need to be implemented in a fashion that allows the smooth operation of the overall network as a singular body. Nevertheless, vast technologies and communication techniques are required to work in unison. An increment in demand of such an efficient system is deemed to attract massive numbers of users utilizing resources simultaneously, which in turn, requires both acquisition and utilization of the spectrum. Some exceptional candidate technologies that enable 5G to better accommodate a large number of users within the limited resource environment are, but not limited to, mmWave, massive multiple-input multiple-output (massive MIMO), multi-radio access technology (RAT), device-to-device (D2D) communication, and cooperative heterogeneous network (HetNet) [2–7].

The requirement of achieving high reliability and low latency for many Internet of Things (IoT) uses is very critical. In this regard, for a new 5G use case, IoT applications are classified into two classes, i.e., massive machine-type communication (mMTC) and ultra-reliable low-latency communication. There are several practical applications that are possible for a 5G IoT network such as: (i) D2D communication without the need of a cellular network; (ii) real-time delay wireless link for medical robots which can help to do remote surgery; (iii) mMTC such as solar-powered streetlights to help citywide infrastructure, and many more. We know that the 5G networks are bound to hit the market soon worldwide [8], and we realize such technology demands simple, but effective and reliable channel models based on basic physics that also derives from extensive testing and measurement. These channel models aid development of various terms of establishing signaling protocols that ascertain efficient utilization of resources, while improving network performance [9]. Various groups have built their own channel models, such as the statistical spatial channel model NYUSIM by the New York University, COST 2100, 3rd Generation Partnership Project (3GPP), International Telecommunication Sector (ITU-R), WINNER II, as well as the Mobile and Wireless Enablers for the Twenty-Twenty Information Society (METIS) [10,11].

Moreover, it is important to highlight that the entire frequency spectrum would not be used up. An average consumer would require centimeter-sized waves with spectrum licenses ranging from 3 to 30 GHz, as well as between 30 and 40 GHz (up to 300 GHz) as a mmWave spectrum, initially [12,13]. There is also spectrum sharing that ranges from 60 to 70 GHz for mission-critical services [14], which includes smart city infrastructure, healthcare, self-driving cars, and many other applications. Such services need a continuous high-speed and low-latency connection, and therefore the shared spectrum is key enabler and ensures that these devices are always connected [15]. For example, termination is absent for the connection between a cellular tower and a self-driving car because some other user may place a call on the same spectrum. Consumer usage is a factor that is emphasized when designing shared spectrum. However, enabling mmWave systems in an ultra-dense network may address issues related to the channel impairments and the propagation range. Nonetheless, some issues need to be mitigated prior to practical implementation. For example, mmWave suffers from high penetration losses that cause a lower transmission range [16]. Moreover, higher frequencies are more easily absorbed by the atmosphere, hence being scattered and absorbed by weather events and buildings, which demand nearly a line-of-sight (LOS) communication [17,18]. It has been predicted that the 5G mmWave would need a massive amount of small-cell deployment, hence the requirement for very small, directive, and high-gain antennas. Besides, free-space propagation is deemed to suffer extremely high attenuation losses due to the small signal wavelength [19]. The design of compact, high-gain, and steerable antennas for 5G devices is another potential challenge in realizing mmWave communication. The direction of the pointing vector of electromagnetic waves, especially for non-line-of-sight (NLOS) environment, is critical to attain maximum quality of service (QoS) performance [20,21].

The 5G network performances are in line with this objective. First, it has a data rate, where 10 Gbps is supported in the cellular area and 1 Gbps at cell-edge, which refers to the location with the worst performance [22,23]. Second, the spectral efficiency has to boost up in order to accomplish 10 bits per second per Hertz [24]. Besides, while achieving higher capacity, it must support more than a million devices after taking into account vehicle IoT, smart devices, wearable devices, and smartphones within a one-square kilometer area [25]. High mobility and very small latency, for example, to support vehicles, trains or aircrafts moving at 300 to 500 kilometers per hour, have to offer end-to-end service upon data request, which requires delivery within 5 milliseconds (ms), whereas from the access point to the device, it should be below 1 ms [26]. In order to accomplish this, the 3rd Generation Partnership Project (3GPP) and the International Telecommunication Union (ITU) is expected to set 5G standards; the 3GPP Release-16 is not expected until 2020 [27,28]. The core technologies under consideration for the 3GPP Releases seem to work on a new waveform design, multi-RAT interworking, exceeding 6 GHz frequency band, massive MIMO antenna configuration, as well as advance D2D and flat network [24].

For the perfect channel condition, the receiver must receive the best signal-to-noise ratio (SNR) value. This is possible when one can receive a transmitted signal without attenuation, loss or noise. However, due to the unpredictable behavior of a wireless channel, the signaling overhead causes various serious issues when the propagation signal is continuously varying. In addition, when we are propagating the signal in a large number of antennas, the multipath propagation system delivers better spectral efficiency with a promising capacity gain [29]. In order to achieve optimal detection, generally, perfect Channel State Information (CSI) is assumed to be between the transmitter (Tx) and receiver (Rx). However, in practice, due to the mobility of the communication environment, the impulse response of the channel varies, thus inducing the need for channel estimation. In addition, permanent feedback signaling is required to notify the estimated CSI at the Tx, and many time slots are engaged during the feedback, thus reducing the bandwidth efficiency of the system. In real-world cellular environments where most users communicate to base stations (BSs) through channels with no LOS path, having access to precise geometric information regarding the relative locations of the BSs and users that yield high spectrum efficiency [30]. Therefore, the propagation behavior of the channel has a vital role in this situation, because the response of the propagation signal can be predicted [31]. Thus, in order to critically study the performance of the future 5G mmWave wireless network, analyzing the features of the propagation channel and its behavior is essential [32]. The aim of any reliable communication is to achieve a reliable (i.e., accurate) transmission link between the Tx and the Rx [33], including path loss, which is a major aspect upon assessing various types of network scenarios [34]. The factors that directly affect path loss are the distance between the source and the user, operating frequency, fading effect, environmental surface, and meteorological conditions [35,36]. Hence, researchers have been employing several probabilistic techniques in modelling various path losses for various noise and interference-limited scenarios, due to the nature of randomness in wireless channels. Experiments and extensive results have attained diverse datasets, and keeping those studies in mind, researchers have designed many path loss models to predict signal attenuation of the propagation channels. Researches are currently exploring radio channels, such as 28, 32, 36, 38, 60, and 73 GHz [37–39]. Some of the latest developments that predict propagation channels are explained in the next section.

In this paper, the propagation channel was estimated by extracting the path loss exponents (PLEs) value at the 38 GHz frequency band. The simulation results were calculated to investigate the potential of mmWave propagation path loss models, such as FI and CI [37,40]. The measurement readings were collected by using a directional horn antenna in an outdoor urban microcell environment for both LOS and NLOS scenarios with co (vertical-vertical) and cross (vertical-horizontal) antenna polarization settings. On the basis of real measurement of path loss parameters, the various network performance parameters, such as average user throughput, fairness index, cell-edge user throughput, and spectral efficiency, as well as average cell throughput, have been examined. The outcomes were also analyzed at various MIMO antenna configurations to enhance the overall achieved network performance. The rest of the paper is organized as follows: Section 2 highlights the most recent and relevant works published

within the same area; the measurement setup, hardware description, and experimental procedure are explained in Section 3; both FI and CI path loss models are discussed in Section 4; the experimental findings of PLEs values are provided in Section 5; simulation setup description is expressed in Section 6; Section 7 depicts the detailed results to evaluate various network performances for a varied number users and MIMO conditions; lastly, the conclusion, along with future work, is discussed in Section 8.

2. Related Work

One key enabling solution for meeting the extreme data demand growth is the utilization of previously unused mmWave frequency spectrum. Although the mmWave spectrum offers a better way to enhance channel bandwidth and network capacity, it also causes various channel propagation issues that must be addressed prior to setting any standards for the 5G spectrum. In order to mitigate these issues, numerous studies have been performed to investigate the behavior of the propagation channel. For instance, in [41], an in-depth survey was conducted with details of various path loss models explained, based on their similarities and differences. This paper categorized more than 50 proposed models into several various groups, such as basic models, supplementary models, fading models, and ray models. Moreover, the authors in [42] presented a simple path loss model, as compared to the ITU indoor propagation model by 3GPP that is currently in use. The authors conducted the experiments at 28 and 73 GHz frequency bands in an ultra-dense indoor office environment. Similarly, a path loss model for large-scale high-density urban scenarios at 28 and 73 GHz frequency bands has been reported in [43]. The "3D ray-tracing" simulation software program was utilized to design the propagation path loss models for the large-scale next-generation network [44–46].

The paper presented in [47] reported a probabilistic omnidirectional propagation path loss model using a probability distribution at the 28 and 73 GHz frequency bands. It applied CI free space reference distance (FSRD) path loss model and FI path loss model. It proposed the probabilistic weighting function that appears helpful for choosing between the best communication link for the LOS and NLOS settings. In [48], the authors investigated the channel at 73 GHz frequency band with directional antennas. Hence, an experiment was conducted in a high-density urban scenario using various combinations of a user's location for mobile and backhaul with more than 30 access points. The authors stated that omnidirectional models suffer from more path loss at higher frequency bands, thus the use of mmWave spectrum, particularly the E-band (71–76 GHz and 81–86 GHz), with the help of beam-combining and beam-steering, which could lead to a usable system for future wireless technologies through the exploitation of multipath in a high-density urban environment.

In [49], the authors presented a channel measurement for RF wideband for both NLOS and LOS peer-to-peer scenarios via narrow beam antennas at 38 and 60 GHz frequency bands. The experiment was conducted using broadband sliding correlator channel sounder and steerable antenna. The outcomes were presented by characterizing the propagation path loss in dB and time delay spread for many real-world scenarios. The antenna-pointing angles relationship and root-mean-square delay spread were analyzed, and showed that the path loss and the distance between sources to destination are linearly proportional to each other. The outcomes proved that the use of a local multipoint distribution system (LMDS) spectrum seemed better in terms of user throughput, transmission time, and power optimization, particularly for the LOS scenario.

Another method in [50] assessed the use of beam forming at 28 and 38 GHz mmWave bands by proposing a new path loss model that employed the industry-standard path loss models with several modifications. It was proven that the use of pointed single best directions for directional antennas could minimize the required number of the 5G BSs, as compared with the arbitrary pointing angles approach for directional antennas. The approach in [51] proposed a height-dependent path loss model for NLOS urban micro outdoor scenarios. The authors utilized omnidirectional antennas and a high-power gain amplifier, which were later compared with the outcomes of 3GPP path loss models at 3.5 GHz. They also investigated the impact of shadowing and penetration losses caused by the human body and herbage environment. The large-scale path loss model was analyzed in [52] by

using co and cross antenna polarizations for directional Tx and Rx antennas, particularly at the 32 GHz frequency band. The study showed that in a comparison of the FI model, the use of CI free space path loss model displayed some limitations in the NLOS environment. As for the propagation channel analysis, the urban measurement campaign was conducted with a synchronous channel sounder system at the 28 GHz frequency channel [53]. This paper investigated the omnidirectional spatial channel model for the NLOS path based on wideband propagation measurements.

The authors in [54] assessed the indoor channel using a 28 GHz multibeam MIMO prototype. The authors performed multibeam forming using continuous aperture-phased MIMO (CAP-MIMO) that utilized a lens antenna array. They claimed to use a first-time simultaneous multibeam channel measurement of about 4° beam width. They also stated that by using a CAP-MIMO transceiver in place of the existing conventional sounder it not only enabled spatial resolution, but also allowed them to practice using the simultaneous multibeam, which enhanced network performance. In the study reported in [55], the investigation achieved the angularly resolved path loss measurement in an urban microcell scenario at the 28 GHz frequency band. The authors stated that most of the signal energy was lost in the NLOS path, as compared with the LOS path. Nevertheless, only a few of the small refraction and reflection objects gave better signal quality, as received for the LOS path. The two similar approaches in [56,57] compared the propagation characteristics of 11, 16, 28, and 38 GHz by utilizing space-alternating generalized expectation (SAGE) maximization to process the measurement data. This study analyzed some new massive MIMO propagation properties, such as spherical wavefront property, cluster birth-death property, and non-stationary over the array, by investigating the variations of channel parameters. Their work showed that these massive MIMO propagation characteristics could be used for large antenna array systems for mmWave channel modelling. Another study in [58] examined the frequency bands at 60 GHz and 73 GHz using the Stanford University Interim (SUI) and standard theoretical free space (FS) path loss models, including their potential ability to deliver performance. The results proved, explicitly, that accounting for the number of beams (or discrete angles) combined at the Rx could result in receiving a strong signal power. An approach in [59] studied the urban microcell wideband measurement at 28 and 38 GHz by using a channel sounder equipped with an omnidirectional and steerable directional antenna. This study characterized various small- and large-scale parameters, such as angular speed, shadow fading, delay spread path loss, and clustering, in order to determine the potential of mmWave frequencies. Their results predicted that the PLEs value of 2.0 for the LOS environment, while, for the NLOS it hit 3.0. They concluded that the LOS PLEs of the UMi environment at 28 and 38 GHz were similar in value to each other and were quite close to the theoretical free space value of 2. Moreover, the large- and small-scale parameters at 28 GHz were similar as achieved at 38 GHz. In [60], the dual-directional path loss model that incorporated both the LOS and NLOS transmissions was proposed. The authors analyzed the results in terms of average data rates achievable and coverage probability. Furthermore, in [61], the access links and backhaul links for D2D communication have been examined, along with their impact due to outdoor path loss models in the presence of solar radio emissions at a frequency band of 60 GHz. The research highlighted that the solar radio emission could be useful in minimizing carrier-to-noise ratio (CNR) and in increasing the corresponding PLE values for path loss channel models with large-scale propagation. The authors in [62] focused on most of the frequency bands between 2 GHz and 26 GHz, apart from studying their relationship between the frequency dependent path loss models in an urban macro-cell scenario. Their results depicted similar dependence in the LOS scenarios, while a relationship of directly proportional was observed in NLOS environment. Another approach in [63] investigated shadowing models that established correlation distances, varied offsets, shadowing, fading variance, and PL slope for the urban street canyon environment of New York City. The proposed model was largely dependent upon huge calibrated raytracing (RT) simulation and the dataset was set with over 60,000 PL data points with a total of 11 varied BS locations. The authors established a path loss model for spatially-consistent stochastic street-by-street (SBS) for a 28 GHz microcell scenario. The results depicted in the paper

proved that the proposed SBS modelling principle scenario performed better after spatial consistency was taken into account. Table 1 illustrates the main findings and the variances of the related work.

Table 1. Related work summary.

Models/Scenarios	Methodologies	Advantages	Important Results	References
Large-scale high-density path loss model for ultra-dense indoor environment	Omnidirectional path loss model with directional antenna are utilizes for 28 and 73 GHz frequency band channel measurement	Utilizing of antenna pointing angles deceases the mean square delay spread	Accurate large-scale path loss model (CI free space) for distance and frequency as compared to existing 3GPP and FI model	[42]
Omnidirectional propagation large-scale path loss for high-density urban scenarios	Utilizing 3D ray-tracing simulators to conduct the experiment at 28, 38, and 73 GHz frequency band for LOS and NLOS scenario	Proposed model already widely been used by known companies (Nokia and Samsung)	Large-scale pathloss models using CI 1 meter free-space reference distance measurements are presented at 28, 38, and 73 GHz	[43]
Probabilistic omnidirectional propagation model for outdoor scenario	Uses CI and FI path loss model at 28 and 73 GHz	Proposes the probabilistic weighting function which is useful for LOS and NLOS determination	Proposed model is useful to estimated coverage, interference and outage	[47]
73 GHz mmWave Propagation measurements for outdoor Urban scenario	E-band propagation measurement for both backhaul and mobile scenario by using directional antennas	Use of beam combining and beam forming lower the path losses	Achieved PLEs values are comparable with current microwave cellular PLEs values	[48]
Angle-dependent peer-to-peer RF wideband channel measurements	Utilizes narrow beam antennas at mmWave carrier frequencies at 38 and 60 GHz for both LOS and NLOS	Higher SNR and low root-mean-square delay is achieved by shaping optimum antenna pointing angle	Tx-Rx distance has an inverse relation on Path loss values	[49]
Modification of industry-standard path loss models	Beam forming at 28 and 38 GHz based on arbitrary pointing angles of directional antennas	Coverage range increases which reduces the required number of the 5G BSs	20 times higher capacity gains as compared to current LTE network	[50]
Height dependent path loss model at 28 and 38.6 GHz	Utilized Omnidirectional antennas and high-power gain amplifier for NLOS urban micro outdoor scenario	The achieved result is better as compared to 3GPP path loss models at 3.5 GHz	Investigates the effect of shadowing and penetration losses caused by the human body and herbage environment	[51]
Large-scale path loss model at the 32 GHz frequency band	Co and cross antenna polarizations for the directional Tx and Rx antenna for CI and FI model	Suggested PLE values for horn-to-horn and horn-to-omnidirectional outlined	CI path loss model shows lower performance as compared to FI path loss models in NLOS scenario	[52]
Wideband spatial Channel propagation analysis at 28 GHz	Investigates the spatiotemporal channel characteristics such as multipath delay, angular statistics and pathloss	Useful for the high-density urban environment	Performed clustering analysis for its power distribution	[53]
New measurement methodology for indoor channel at 28 GHz	Multibeam forming using continuous aperture phased MIMO (CAP-MIMO)	It achieved spatial resolution, freedom to simultaneous multibeam and improved network performance	Four electronically selectable beams can simultaneously measure four spatial channels	[54]
Highly directional path loss measurement for urban microcell scenario at 28 GHz frequency band	Angularly resolution path loss measurement for both azimuth and elevation polarization	Provide better signal quality as received for LOS path	Small and specular objects reflecting causing more energy loss	[55]
Propagation characteristics at 11, 16, 28, and 38 GHz mmWave frequency band	The space-alternating generalized expectation (SAGE)- maximization algorithm is applied to obtain multipath component	Validated to use of large antenna array system for mmWave channel modelling	It investigates the spherical wavefront, cluster birth-death and non-stationarity property over the antenna array	[56,57]

Table 1. *Cont.*

Models/Scenarios	Methodologies	Advantages	Important Results	References
Standard theoretical free space (FS) and Stanford University Interim (SUI) path loss model at 28, 60 and 73 GHz	Number of beams (or discrete angles) combined at the Rx, can result in strong received signal power	Strong achieved power signal in adaptive array systems	It provides generalized beam combining model for mmWave path loss prediction	[58]
Urban microcell wideband at 28 and 38 GHz	Using channel sounder equipped with omnidirectional and steerable directional antenna	Characterizes path loss, shadow fading, delay spread, angular spread and clustering parameters	PLE for LOS case in 2 and for NLOS case in 3 and similar large- and small-scale parameters achieved at 28 and 38 GHz	[59]
Blockage effect causes low coverage for small cell networks	Dual-directional path loss model incorporates for both LOS and NLOS transmissions	Higher Coverage probability and better average achievable rate	Higher BSs and lower blockages intensity cause lower average achievable rate	[60]
Outdoor propagation path loss models at 60 GHz bands	Investigates the effects of solar radio emissions for access/backhaul links and D2D communications	This study helps to prepare appropriate link budgets for deploying 60 GHz for hot and sunny weather	Results shows 9 to 15.6% higher PLE values in hot sunny weather (41–42°) as compared to cool night weather (20–38°)	[61]
Measurement at 2 to 26 GHz in an urban macro cell environment	Path loss frequency dependence is investigated	Dependence is similar in LOS areas	Larger frequency dependence is found for NLOS environment	[62]
Spatially consistent street-by-street path loss model for the 28 GHz microcell scenario	Model is based on large calibrated raytracing (RT) simulation dataset of 11 BS locations and over 60,000 PL data points	Achieve better spatial consistency	Different shadow fading, PL slope, variance, correlation distance, offset for each street	[63]

3. Measurement Setup

In order to model the future 5G wireless propagation channel, the co- and cross-polarization antennas setup was employed in this work. The 38 GHz radio signal was transmitted and measured at various Tx-Rx separation distances to determine the parameters for large-scale path loss. Data were gathered at the park beside the Registrar office located in UTM Kuala Lumpur campus. This environment emulated the older environment of the hostel that contained the old-fashion building with only two floors, while the park was situated in the middle, as depicted in the captured image illustrated in Figure 1a. In this scenario, the Tx and Rx were fixed at 18° half-power beam width (HPBW) in the elevation and azimuth planes via a narrowband continuous wave (CW) signal generator to generate 30 GHz mmWave frequency signal. Two varied sets of data, up to 50 m, for the LOS and NLOS cases were captured, respectively, as illustrated in Figure 1a,b. The Tx was set on a 5-m antenna mast on the ground floor (identical location for the access point of the outdoor environment), while the Rx was strapped on a column at a height of approximately 1.7 m. Measurements of varied combinations for a total of 30 Tx-Rx pairs were examined in both cases of the NLOS and LOS scenarios. The calculation complexity and simulation time of shooting and bouncing rays (SBR) method was proportional to the number of devices and objects presented in an environment. Because of the higher reflection and diffraction of mmWave signals in an urban environment, the use of highly directional horn antenna was preferred to achieve an acceptable output at the user end [64]. Therefore, these measurements were performed using the directional narrow-beam Rx antenna with a 3D transmitter-receiver separation distance varying between 20 and 50 m. In order to create a LOS link between the transmitter and the receiver for the LOS scenario, both antennas were boresight aligned with high directivity to each other and no obstacle between them. Moreover, for the NLOS, both the transmitter and the receiver were separated by buildings, such that no LOS link was established and both Tx and Rx antennas were directed towards each other at the corner of the building (yellow and red arrows show the direction of antennas, as shown in Figure 1c, to point out the complete measurement scenario from the top view).

(a) (b)

(c)

(d) (e)

Figure 1. (**a**) line-of-sight (LOS) environment, (**b**) non-line-of-sight (NLOS) environment, (**c**) measurement scenario, (**d**) signal generator, (**e**) signal analyzer.

3.1. Hardware Description

The radio frequency signal was transmitted by using an Anristu MG369xC signal generator (with Pt = 9 dBm) through a wireless channel and was captured by a narrow-band horn directional antenna at the Rx side, in order to present the directional propagation path loss model. At the Tx side, the continuous radio wave was generated by using an Anritsu MG369xC Series synthesized signal generator device (see Figure 1d), which was connected to a highly directional horn antenna.

On the other side (i.e., Rx), the received power level was captured using an Anritsu MS2720T handheld spectrum analyzer (see Figure 1e), which was operated at zero spans with 50 ms sweep time connected to the horn antenna. The noise contribution was –85 dBm/Hz when the resolution channel bandwidth (RBW) of the spectrum analyzer was set to 100 kHz at a 38 GHz frequency setting.

3.2. The Experimental Procedures

In order to characterize the mmWave channel, two different antenna polarizations were used, i.e., vertical-horizontal (V-H) and vertical-vertical (V-V) for both the LOS and NLOS environments. In order to verify the precision and to confirm the experimental outputs, the measurement results were verified five times for a specific environment. As for the LOS measurements, the transmitter and receiver were realigned at the clear-cut point, and using the laser pointer both were aligned at the same azimuth and elevation angles to ensure that the boresight of both the transmitter and the receiver were pointing to each other. In order to minimize the random errors for each scenario, the measurements were fixed at 100–200 samples/reading period. The recorded data were stored in an internal storage of the spectrum analyzer, which were later transferred to the PC for successive processing. Both Tx and Rx were rotated in the x-y plane at azimuth angles of −20°, 0°, and +20°. As for the LOS characterization, the Rx was placed at 1 m from Tx and then the measurement points were collected in increments with a 5-m gap between each subsequent reading point, up to 50 m (see Figure 1a). In the NLOS, the measurements were scaled up to 50 m, while the Rx was placed at a minimum distance of 20 m, as a starting point, to achieve a perfect NLOS scenario, and then recorded the measurements starting from 50 m with a 1-m gap (see Figure 1b).

4. Large-Scale Path Loss Models

The purpose of path loss modelling is to evaluate the magnitude of attenuation experienced by broadcasting radio signals over a distance, which is useful for designing communications systems. In order to determine the received signal strength at Rx, a large-scale path loss was utilized between Tx and Rx for both the LOS and the NLOS environments. The path loss model is commonly used to illustrate the channel effects caused by the surrounding environment. It can predict whether the path loss prediction model should be based on theoretical (deterministic), empirical (statistical), or a combination of both methods [65]. However, the ideal channel prediction can be achieved when the path loss model is designed from real-time practical measurements [66]. It differs for varying communication systems, while radio channels can be modelled in a statistical fashion. The path loss formula provided the Friis free space equation can be used for the reference point or measured at distance d_0. The conditions assumed for this model attempted to replicate real-life readings from the experiments but could never guarantee a perfect match due to the random nature of obstructions, aerodynamics of buildings depending on weather, reflections from the buildings and ground, as well as terrestrial communication. Thus, in this paper, the two most potential path loss models (CI free space and FI path loss) for the 5G network have been considered. [67,68]. The CI model is easily implemented in existing 3GPP models by making a very subtle modification, that is by replacing a floating non-physically based constant with a frequency-dependent constant that represents free space path loss in the first meter of propagation. This model is most suitable for outdoor environments because of its accuracy, simplicity, and superior sensitivity performance due to its physical close-in free-space reference point, given the fact that measured path loss exhibits little dependence on frequency in outdoor environments beyond the first meter of free-space propagation. The CI model relies on a FSRD of 1 m standard value, where its path loss model is expressed in Equation (1) with the presence of a single model parameter, n, which is also stated as the path loss exponent (PLE). The path loss in dB as a function of 3D T-R separation distance, d, and the carrier frequency f, is expressed as:

$$PL^{CI}(f,d)[dB] = FSPL(f,d_0) + 10n\log_{10}(\frac{d}{d_0}) + \chi_{\sigma}^{CI} \quad (1)$$

where the free space path loss of the anchor point is given by:

$$FSPL(f, d_0) = 20\log_{10}\left(\frac{4\pi d_0 f}{c}\right) \tag{2}$$

and the large-scale signal fluctuations resulting from large obstacles in the surrounding environment were embedded in the model by the shadow factor, χ_σ^{CI}, which is a zero mean Gaussian random variable written as:

$$\chi_\sigma^{CI} = PL^{CI}(f, d)[dB] - FSPL(f, d_0) - 10n\log_{10}\left(\frac{d}{d_0}\right) \tag{3}$$

while its standard deviation, σ^{CI}, in dB is:

$$\sigma^{CI} = \sqrt{\frac{\sum\left(\chi_\sigma^{CI}\right)^2}{N}} \tag{4}$$

denotes the overall number of measured points in the measurement campaign [69].

The best fit minimum mean square error (MMSE) of the PLE n and the minimum standard $\sigma_{\min}^{CI}$ deviation were calculated as in (5) and (6), respectively.

$$n = \frac{\sum\left(PL^{CI}(f, d)[dB] - FSPL(f, d_0)\right)\left(10\log_{10}\left(\frac{d}{d_0}\right)\right)}{\sum\left(10\log_{10}\left(\frac{d}{d_0}\right)\right)^2} \tag{5}$$

$$\sigma_{\min}^{CI} = \sqrt{\frac{\sum\left(PL^{CI}(f, d)[dB] - FSPL(f, d_0) - 10\log_{10}\left(\frac{d}{d_0}\right)\frac{\sum\left(PL^{CI}(f,d)[dB] - FSPL(f,d_0)\right)\left(10\log_{10}\left(\frac{d}{d_0}\right)\right)}{\sum\left(10\log_{10}\left(\frac{d}{d_0}\right)\right)^2}\right)^2}{N}} \tag{6}$$

Another path loss model, which was adopted by WINNER II and 3GPP standardization bodies [67], and the FI path loss model, also known as the alpha-beta model, were employed in this study. This model did not consider the anchor point, and therefore it was not physically-based. The path loss in dB based on the FI model as a function of the 3D T-R separation distance d is given by [47].

$$PL^{FI}(d)[dB] = \alpha + 10\beta\log_{10}(d) + \chi_\sigma^{FI} \tag{7}$$

where α denotes the FI in dB, β refers to a coefficient referred to as line slope that characterized the distance dependency of the path loss, χ_σ^{FI} is defined as a zero mean Gaussian random variable that stands for shadow factor, and σ^{FI} signifies the shadow factor standard deviation in decibels.

In order to minimize the standard deviation, σ^{FI}, using the MMSE technique, it is required to solve for α and β values to determine the best minimum error fit, as follows:

$$\alpha = \frac{\sum 10\log_{10}(d)\sum 10\log_{10}(d)PL^{FI}(d)[dB] - \sum\left(10\log_{10}(d)\right)^2 PL^{FI}(d)[dB]}{\sum\left(10\log_{10}(d)\right)^2 - N\sum\left(10\log_{10}(d)\right)^2} \tag{8}$$

$$\beta = \frac{\sum 10\log_{10}(d)\sum PL^{FI}(d)[dB] - N\sum 10\log_{10}(d)PL^{FI}(d)[dB]}{\sum\left(10\log_{10}(d)\right)^2 - N\sum\left(10\log_{10}(d)\right)^2} \tag{9}$$

$$\chi_\sigma^{FI} = PL^{FI}(d)[dB] - \alpha - 10\beta\log_{10}(d) \tag{10}$$

and the standard deviation is calculated as:

$$\sigma^{FI} = \sqrt{\frac{\sum\left(PL^{FI}(d)[dB] - \alpha - 10\beta\log_{10}(d)\right)^2}{N}} \quad (11)$$

5. Experimental Results

The CI model always displayed a physical equivalence and continuous relationship between the distance and the transmitted power due to CI free-space anchor point [68]. In the result section, d_0 = 1 m was applied, as this distance has been considered as a standard reference in published work since it allows the measurement of path loss to transmit power of the CI model [70]. Table 2 shows the comparison of the CI model parameters for the LOS and NLOS environments. The PLE values were 3.0990 dB and 4.2556 dB for co-polarization and cross-polarization, respectively. The shadowing factor (SF) was 9.2268 dB by using a 1-meter FSRD for co-polarization, and 8.3041 dB for cross-polarization. The cross-polarization factor (XPF) was calculated as defined in Equation (3) of [46]. The fitting of the PLE n at 38 GHz for both co- and cross-polarizations are displayed in Figures 2 and 3, respectively. On the other hand, the FI model (see Table 3) shows the path loss parameters: α = 75.1359, β = 2.3401, and SF= 9.0714 dB for co-polarization, whereas it shows α = 97.6545, β = 1.9560, and SF = 6.5463 dB for cross-polarization. Figures 4 and 5 illustrate the best fitting draw for both co- and cross-polarizations, respectively. Note that, the NLOS V-V and NLOS V-H outcomes were very much correlated for FI model, hence the discussion is only focused on the NLOS V-V case, as described in Sections 6 and 7. It is worth mentioning that these results are comparable to the results reported in [71]. As for the CI model, it is concluded that the cross-polarization decayed faster than the co-polarization for LOS environment, which is similar for the FI model, while cross-polarization exhibited higher path loss value than co-polarization by approximately 20 dB, as portrayed in Figures 4 and 5.

Table 2. Close-in (CI) model summary for LOS and NLOS environment.

Env.	Pol.	PLE	$d_o(m)$	σ (*dB*)	|XPF|
LOS	V-V	3.0990	1	9.2268	0.9227
	V-H	4.2556	1	8.3041	
NLOS	V-V	4.3202	1	7.5277	0.0111
	V-H	4.2914	1	7.5388	

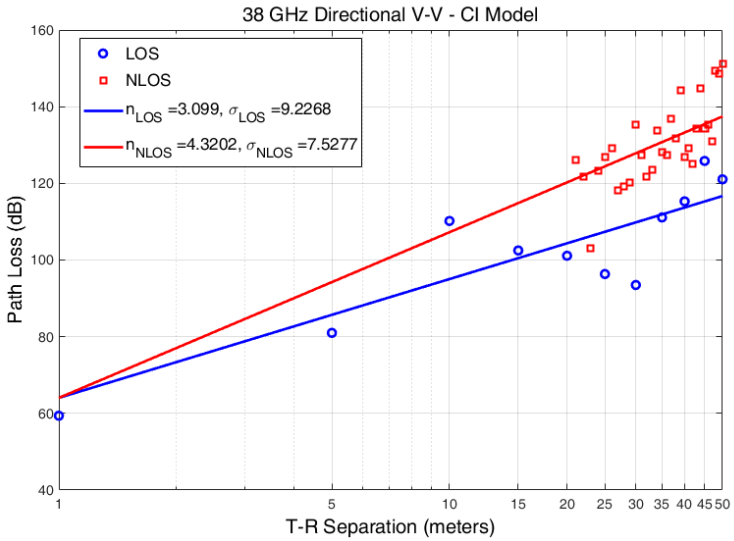

Figure 2. LOS and NLOS CI path loss model for the co-polarization.

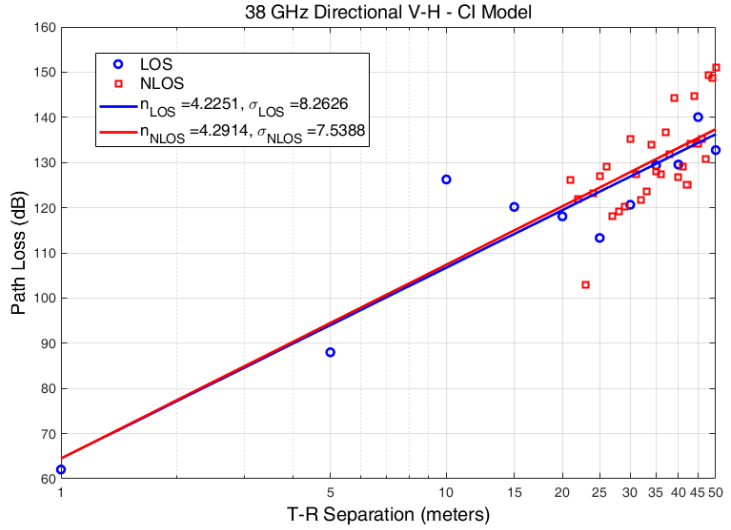

Figure 3. LOS and NLOS CI path loss model for the cross-polarization.

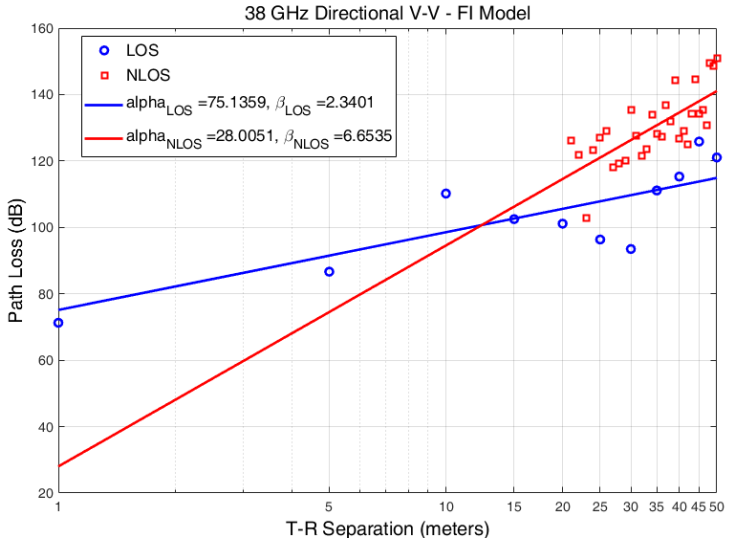

Figure 4. LOS and NLOS FI path loss model for the co-polarization.

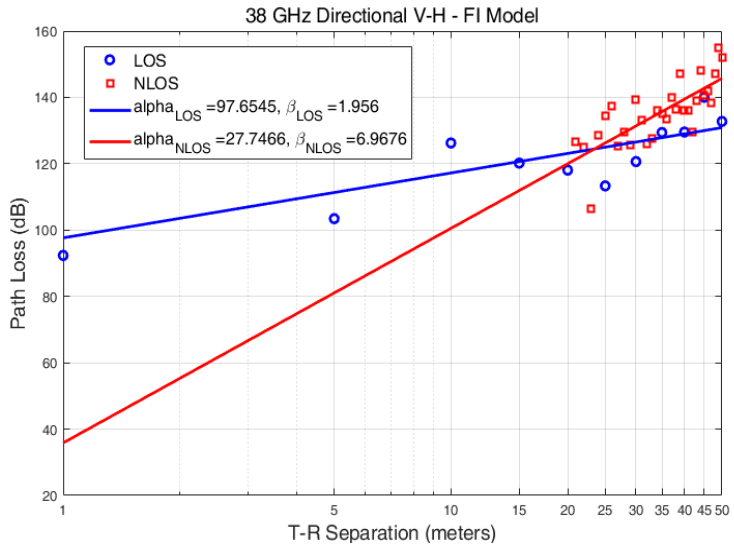

Figure 5. LOS and NLOS FI path loss model for the cross-polarization.

Table 3. Floating-intercept (FI model) summary for LOS and NLOS environment.

Env.	Pol.	β	α	σ (*dB*)
LOS	V-V	2.3401	75.1359	9.0714
	V-H	1.9560	97.6545	6.5463
NLOS	V-V	6.6535	28.0051	7.0683
	V-H	6.9676	27.7466	6.9574

6. Simulation Setup

In this section, the overall network performance was examined in a MATLAB simulation by designing the replica in a real environment based on our practical findings tabulated in Tables 2 and 3. Here, several simulations were performed to investigate the performance of the varied propagation conditions, such as LOS V-V, LOS V-H, and NLOS V-V polarizations for both CI and FI propagation models. As discussed in Section 5, the NLOS V-V and NLOS V-H outcomes were very much correlated, and therefore the discussion only highlights the NLOS V-V case for the simulation outputs. The Monte Carlo technique was used in MATLAB to evaluate the findings and averages were performed over 1000 independent channel realizations. In each cell, the number of users was altered from 10 to 50 and was randomly spread over a coverage area of a cell. Both FI and CI propagation path loss models were used to create real scenarios with the LOS and NLOS environments [72]. It was recommended in [73] that transmission power for each next generation NodeB (gNB) was fixed at 46 dBm with an available bandwidth of 40 MHz at a 38 GHz frequency band. The proportional fair scheduling (PFS) algorithm was used for the coordination between the gNBs. The closed-loop spatial multiplexing (CLSM) transmission mode was employed for 2×2, 2×4, 4×2, and 4×4 MIMO antenna configurations, while the eight layer spatial multiplexing transmission mode was employed for 8×2 and 8×4 MIMO antenna configurations, as defined in [74]. In order to create the effect of heavily built-up ionospheric urban environments, the Rayleigh fading channel was weighed in [75]. There were 21 gNBs in the network with a separation distance of 200 m, as it was the expected cell size for the 5G radio access network [8]. The coupling loss was fixed at 70 dB, as recommended in Section 14.1.2.3 of [76]. The various simulation parameters, along with their certain values, are listed in Table 4.

Table 4. Simulation parameters.

Parameters	Values
Operating frequency	38 GHz
Channel bandwidth	40 MHz
Number of resource blocks	200
No. of users per cell	[10, 20, . . . , 50]
No. of BSs	21
Network scenario	Urban (random user deployment)
CI propagation model	Table 2. PLE (3.0990 for LOS V-V, 4.2556 for LOS V-H, 4.3202 for NLOS V-V)
FI propagation model	Table 3. (β is 2.3401 & α is 75.1359 for LOS V-V, β is 1.9560 & α is 97.6545 for LOS V-H, β is 6.6535 & α is 28.0051 for NLOS V-V
Network geometry	Regular hexagonal grid
gNB Transmission power	46 dBm
Antenna type	Tri-sector tilted
User's speed	5 kmph
No. of Tx	2
No. of Rx	2
Scheduling algorithm	Proportional fair scheduling
No. of iteration	1000
UE height	1.7 m
gNB antenna height	5 m
Transmission mode	Closed loop spatial multiplexing (CLSM) and eight layer spatial multiplexing
gNBs separation	200 m
Fading model	Rayleigh fading
Coupling losses	70 dB

The flowchart illustrated in Figure 6 explains the development of the system simulation.

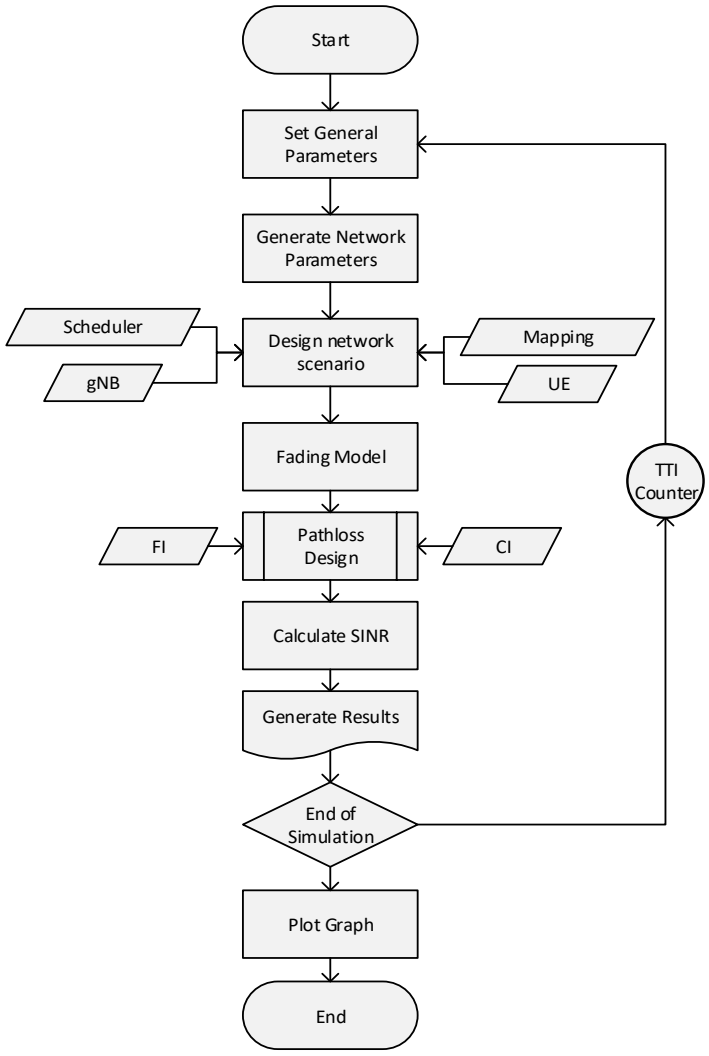

Figure 6. Flowchart of system simulation.

7. Simulation Results

There are various studies that have been conducted which focused on improving the QoS parameters for the wireless network. Such as, the studies in [77,78] that focused on the efficient power control in the uplink of a code-division multiple access (CDMA) wireless network, where it focused on various QoS prerequisites. The corresponding non-convex utility-based multi-service optimization problem was solved by using the game-theoretic framework. The results were evaluated in terms of the user actual and average throughput rate and power consumption. Also in [79], the authors estimated the throughput for their proposed interference management scheme for small cell network. The results were calculated in terms of cell-edge user throughput and outage probability. However, a study focused on channel modeling and considered the effect of fog, rain, and snow during the communication, especially in free space optical (FSO) links [80]. Another study in [81] focused on QoS performance evaluation over the 5G network for an indoor environment. The results of this research are focused on estimating the average cell and user throughputs. Similarly, this section describes the outcomes tabulated by estimating the throughputs of cell-edge users, average cell, and average users, along with fairness index and spectral efficiency for a varied number of users. The performance at various MIMO antenna arrangements, as well as at different channel bandwidths, are also presented for both CI and FI models.

The average user throughput is defined as the amount of data received by a connected user on average in a cellular network. Mathematically, it can be defined as the number of packets received by a specific user [82]. Figure 7 illustrates the outcome of the average user throughput for a varied number of users. It displays the highest cell throughput for 10 users and the lowest cell throughput for 50 users, for all scenarios. As noted, both CI-LOS V-V and FI-LOS V-V scenarios predicted the highest average user throughput for a varied number of users, i.e., 25 and 22 Mbps for a minimum of 10 users, as well as 5 and 4.90 Mbps for a maximum of 50 users. This resulted because the best modulation and coding scheme (MCS) index values were obtained due to the better-received signal quality from both the LOS path and similar antenna polarization. The LOS V-H case for the CI and FI models achieved 17.50 and 12 Mbps for 10 users, while 4 and 3.30 Mbps for 50 users, respectively. On the other hand, the NLOS environment received the lowest throughput for both the CI and FI models, as compared with the LOS case, which was due to the lower power levels at Rx that gave less space for accurately picking the transmission signal.

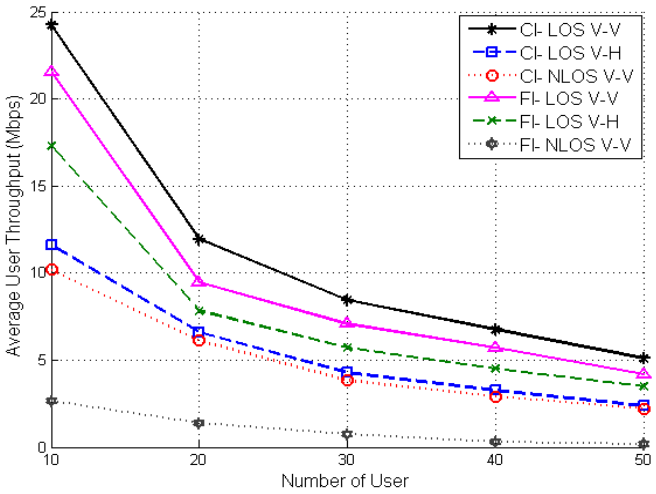

Figure 7. Average user throughput vs number of users.

The cell-edge user throughput was heavily dependent on the strength of the signal received and the number of interferences (co-channel interference (CCI) and inter-cell interference (ICI)), which cell-edge users faced from adjacent cells [23]. Figure 8 illustrates the estimated cell-edge user throughput with respect to a varied number of users. As noted, the cell-edge user performance declined with the increment in the number of users due to the high penetration losses that led to limited resource blocks (RBs) at the user's end. Both CI-LOS and FI-LOS path loss models for V-V polarization were the highest throughput, at 12.10 and 10.80 Mbps for 10 users, respectively. Similarly, for a maximum of 50 users, the cell-edge user throughput for both models reduced and recorded at approximately 3 Mbps. The FI-LOS V-H configuration also forecasted decent throughput for all the users. It estimated 8 Mbps for 10 users and decreased to as low as 1.90 Mbps for 50 users. In contrast, the CI-LOS V-H and NLOS V-V for both CI and FI models predicted the worst cell-edge performance, the data rates were below 1 Mbps for 10 users and even reached a zero signal when the number of users was higher. This result is because the cell-edge users suffered from more ICI and CCI that led to more losses and lowered the channel quality indicator (CQI) value, which caused an ambiguous received signal and low throughput rate.

The average cell throughput depended on the number of active users present in the coverage of users in the cell. Figure 9 illustrates the outcome of average cell throughput for a varied number of users. As discussed in Figures 7 and 8, the CI-FOS V-V predicted the best network performance among all the different model configurations. Consequently, the average cell throughput for CI-LOS V-V forecasted the highest value which was up to 70 Mbps for 10 users and reached a maximum of 90 Mbps

for 50 users. The FI-LOS V-V arrangement forecasted decent performance as well, and reached 65 and 77 Mbps for 10 and 50 users, respectively. Furthermore, FI-LOS V-H also predicted a significant throughput at 65 Mbps for the minimum case of 10 users, and increased up to 13% at an estimated 78 Mbps for a maximum number of 50 users. Moreover, CI-LOS V-H and CI-NLOS V-V achieved moderate values of cell-edge data rate ranging from 30 to 40 Mbps for minimum and maximum cases. On the other hand, FI-NLOS V-V suffered from the minimum data rate, while overall throughput ranged from 5 to 12 Mbps for the minimum to maximum number of users, respectively. Besides, it has been clearly stated that the FI-NLOS case experienced distress from more signal losses with respect to distance and obstacle, which resulted in less average cell throughput.

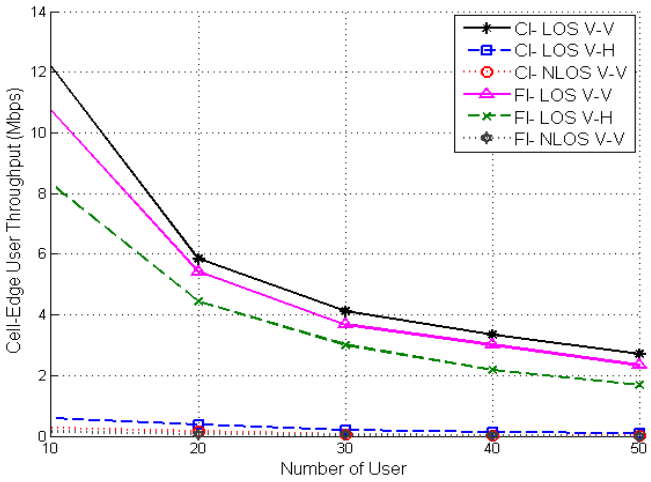

Figure 8. Cell-edge user throughput vs number of users.

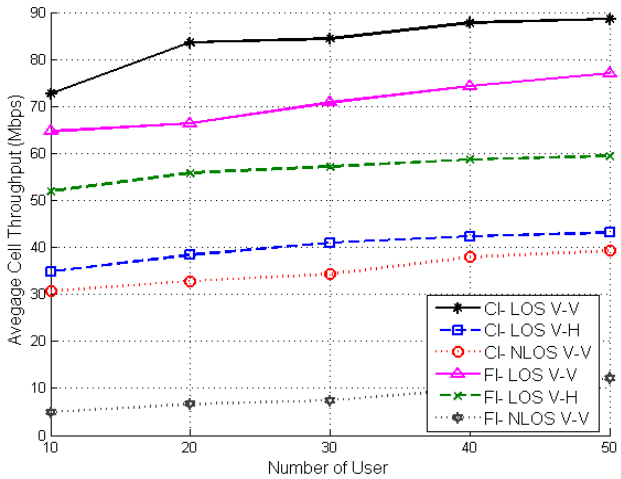

Figure 9. Average cell throughput vs number of users.

To calculate the fairness index that shared the RBs with proper fairness among active users the proportional fair scheduling (PFS) algorithm was applied [83,84]. Figure 10 illustrates the results of the fairness index for the varied number of users. The fairness index for LOS V-V for both CI and FI models hit up to 90%, which clearly displays better CQI with fair RBs distributions. Additionally, the CI-LOS V-H estimated greater fairness for a smaller number of users, but also when a greater number of users were present in a cell. Moreover, in CI-NLOS V-V case, the fairness index was on a slightly lower end, when compared to the CI-LOS V-H case. The NLOS users for V-V case of FI model received a minimum fairness of 13 to 30%, along with the lowest to a higher number of users, respectively. This is due to unfair resource sharing because of poor receiving signal quality caused by the position of NLOS channel between Tx and Rx.

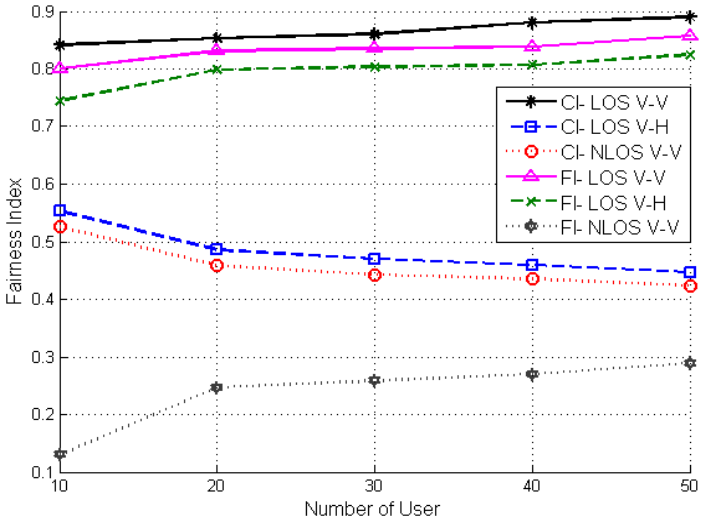

Figure 10. Fairness index vs number of user.

It was possible to achieve spectrum efficiency by increasing the number of users to a maximum limit in a cell while keeping the QoS at an acceptable level. In precise, the given bandwidth was used effectively if maximum information can be transmitted over it [85]. Figure 11 illustrates the outcomes for spectral efficiency for the varied numbers of users. As noted, CI-LOS V-V displayed the highest spectral efficiency between 2.20 and 2.60 b/s/Hz for both minimum and maximum number of users, respectively. This showed the better utilization of given available spectrum by the CI-LOS V-V approach than the other all models. However, FI-LOS V-V also predicted the decent spectrum efficiency of 1.80 b/s/Hz when the number of users was 10, while 2.20 b/s/Hz for 50 users. Additionally, FI-LOS V-H, CI-LOS V-H, and CI-NLOS V-V gave correlated values for both minimum and maximum number of users. For instance, FI-LOS V-H values ranged from 1.50 to 1.75 b/s/Hz, CI-LOS V-H values changed from 1.35 to 1.65 b/s/Hz, and CI-NLOS V-V gave a variation of 30% from 1.20 to 1.60 b/s/Hz for minimum and maximum number of users. Lastly, FI-NLOS V-V estimated the least efficient results i.e., 0.55 b/s/Hz and 1.15 b/s/Hz for 10 and 50 users, respectively. This was because the simulation results based on the FI model displayed greater dependence on the number of users and distance parameter that seemed inefficient for this case, while NLOS path failed to deliver the required data rate, hence resulting in poor achieved spectral efficiency.

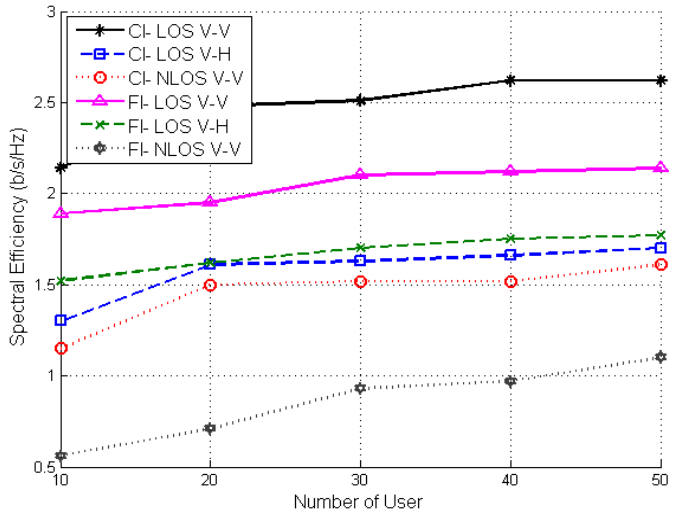

Figure 11. Spectral efficiency vs number of users.

In high-density mmWave network, users tend to face several issues, such as interferences and fading, which minimizes the overall network performance. Currently, several varying techniques are in progress to overcome this issue. The use of a multiple antenna approach is an efficient way to resolve this issue, which not only helps to increase each user throughput, but also enhances the overall network performance [86,87]. For our study, Figures 12 and 13 illustrate the overall network performance of the CI and FI models at various antenna configurations, respectively. We compared the yields for fairness index, spectral efficiency, cell-edge user throughput, average user throughput, peak user throughput, and average cell throughput with respect to varying MIMO antenna configurations. The same CI and FI path loss models, as defined in Equations (1) and (7), were used to calculate the path losses. All other experimental parameters were similar to those specified in Table 4, except for the number of users which had been fixed at 30 and used the LOS V-V formation, which meant PLE = 3.0990 for CI path loss model, as stated in Table 2, whereas β was 2.3401 and α was 75.1359 for the FI path loss model, as outlined in Table 3. Figure 12 portrays the CI propagation path loss model performance, where the 2×2 antenna configuration obtained the minimum and the 8×2 antenna setting attained the maximum overall system performance. In Figure 12a, the fairness indices for all cases were quite correlated, while 2×4, 4×2, and 8×2 delivered better performances of 5, 7, and 9%, when compared to 2×2, 4×4, and 8×4 antenna array settings, respectively. The amount of cell-edge user throughput increment was also observed in Figure 12a with respect to more antenna array settings. However, the cell-edge user throughput improved by almost 100% (i.e., 4.11 to 8.24 Mbps) if we changed from the 2×2 antenna setting to the 8×4 antenna setting. The analysis of the spectral efficiency improved exponentially by approximately 40% from the minimum antenna setting to the maximum antenna array pattern. In Figure 12b, the peak user throughput is also presented, in which the 8×4 MIMO condition obtained 60% more data rate, when compared to the minimum 2×2 antenna settings. Moreover, the average user throughput comparison is illustrated, which gave a minimum value of 8.44 Mbps at the 2×2 antenna array and an increase of 80% to a maximum value of 14.25 Mbps at the 8×4 antenna array setting. Similarly, for average cell throughput, the maximum performance was achieved for the 8×4 configuration (i.e., 142.46 Mbps), which achieved almost 82% higher average cell throughput, as compared with the 2×2 configuration (i.e., 84.42 Mbps).

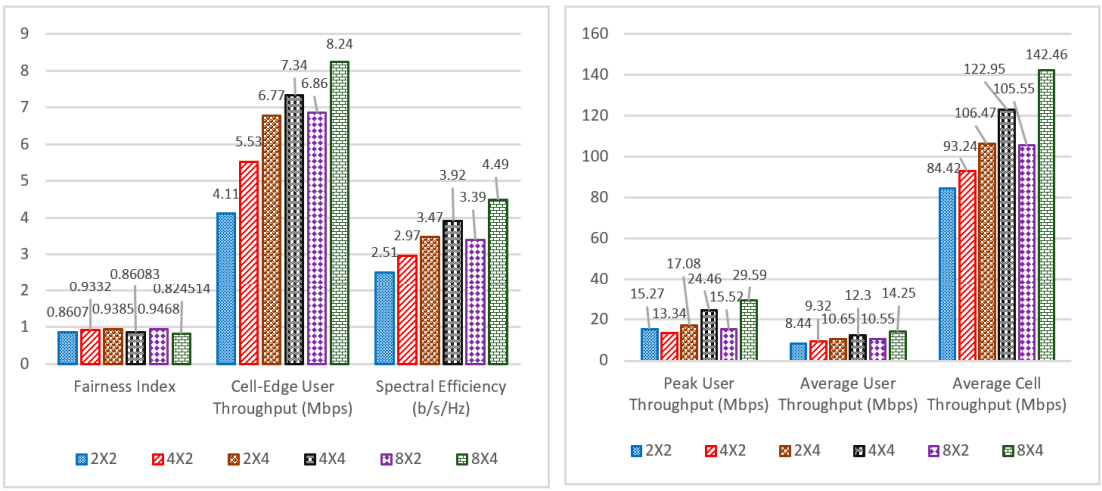

(a) (b)

Figure 12. Overall network performance for CI model at various antenna configurations.

In contrast to earlier findings for the CI model, the overall network performance for FI-LOS V-V case was as illustrated in Figure 13. In Figure 13a, the fairness index was calculated for various MIMO antenna array conditions. The results ranged from a minimum of 0.8348 for 2×2 to a maximum 0.9403 for 8×2 antenna settings. The use of the PFS algorithm displayed similar time, hence allowing all users

at least a minimum QoS, however, due to its limitation on the number of users, the fairness index value fluctuated with the number of users. The cell-edge user throughput is also illustrated in Figure 13a, which showed a similar response to that described in Figure 12a. Here also, the 8 × 4 antenna array achieved the best signal quality and a high cell-edge data rate of 7.63 Mbps, as compared with the 2 × 2 antenna configuration that showed 3.67 Mbps only. Furthermore, the spectral efficiency for the FI model is also shown in Figure 13a for varied antenna patterns. It predicted 2.10 b/s/Hz for the 2 × 2 array and then increased proportionally with respect to more antenna arrays, hence providing up to 75% enhancement for the 8 × 4 antenna array that gave 3.67 b/s/Hz. In a similar way as in Figure 12b, Figure 13b shows peak user, average user, and average cell throughput for varying MIMO conditions. The peak user throughput hiked from a minimum of 10.41 Mbps for the 2 × 2 antenna settings and predicted up to a maximum of 22.26 Mbps for the 8 × 4 antenna array case. Similarly, the average user throughput exponentially increased with more antenna array configurations. A minimum of 7.08 Mbps was attained at the 2 × 2 antenna array and increased to 11.38 Mbps for the 8 × 4 antenna case. Lastly, the average cell throughput is illustrated, which showed a massive improvement of 60% from the minimum for the 2 × 2 antenna setting (which achieved 70.84 Mbps) to the maximum for the 8 × 4 antenna formation (which approximated 113.85 Mbps). Thus, more MIMO configuration led to extra propagation paths between Tx and Rx, which gave better received signal quality, apart from achieving more throughput for the cell users.

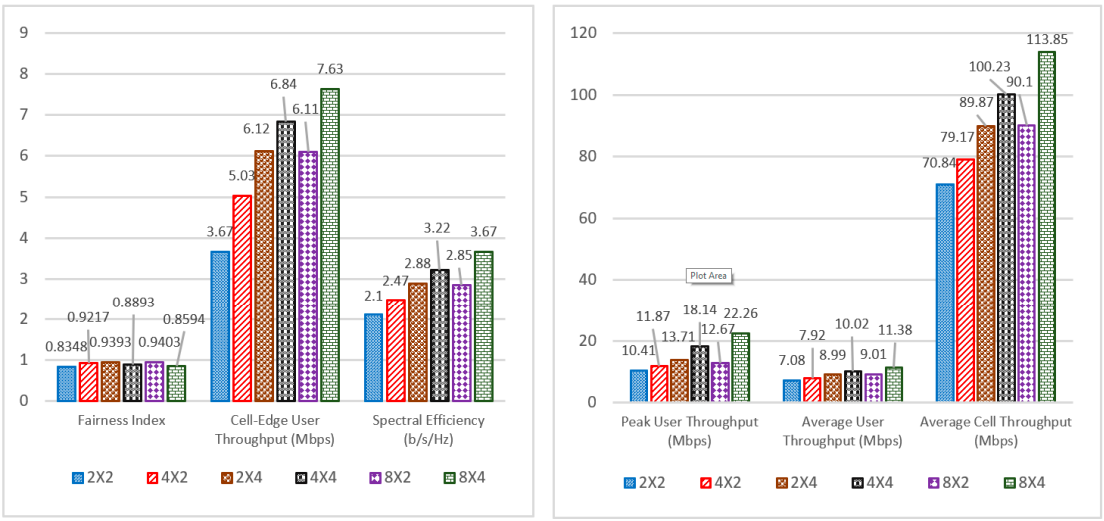

(a) (b)

Figure 13. Overall network performance for FI model at various antenna configurations.

The most important reason for using the mmWave spectrum is to achieve a large bandwidth. Here, Figures 14 and 15 display the overall network performances of the CI and FI models at varying bandwidth settings, respectively. It presents the outcomes for fairness index, average cell throughput, cell-edge user throughput, peak user throughput, average user throughput, and spectral efficiency with respect to different MIMO antenna configurations. All the simulation parameters are similar in appearance to those tabulated in Table 4, when the antenna configuration was set at 2 × 2. On the basis of the data shown in Figures 14 and 15, the user throughputs increased drastically with increments in bandwidth, which indicated that more users would gain higher spectrum sharing in order to transmit information. The fairness index for various bandwidth settings also changed slightly, from 86 to 92% for the CI model and from 83 to 94% for the FI model, as increments in the bandwidth affected the spectrum sharing amongst the users. Spectral efficiency also increased with respect to bandwidth setting as higher spectrum gave extra propagation channel between Tx and Rx, which yielded better received signal quality.

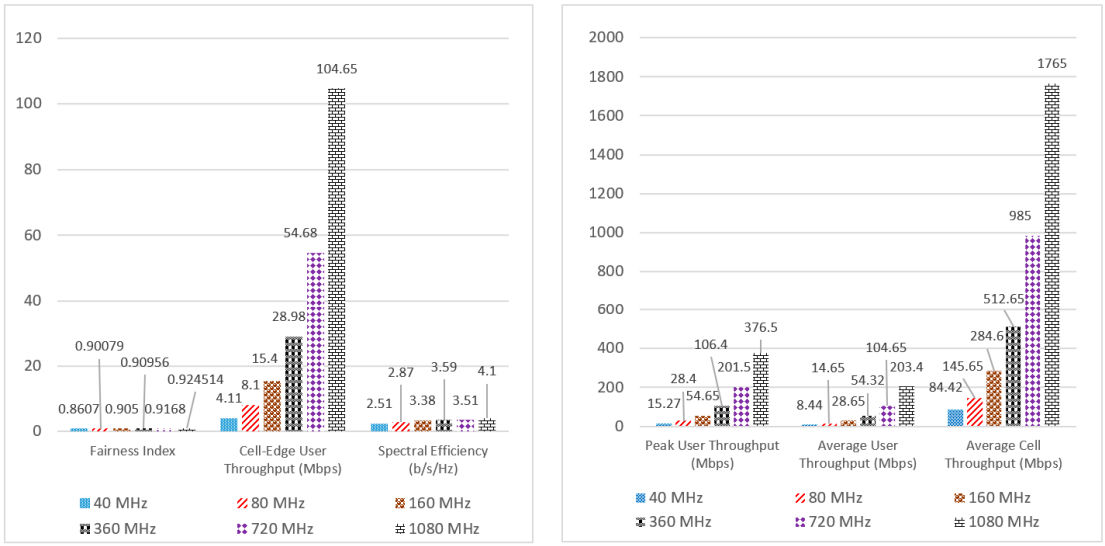

(a) (b)

Figure 14. Overall network performance for CI model at different bandwidths.

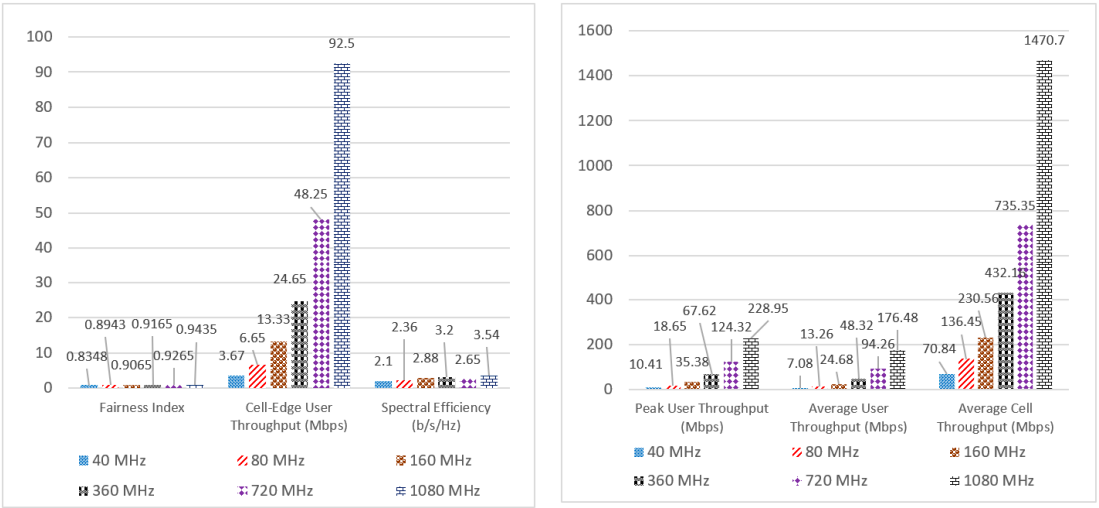

(a) (b)

Figure 15. Overall network performance for FI model at different bandwidths.

8. Conclusions

Recent advancement in technologies has urged 5G developing organizations to work on the mmWave frequency spectrum in order to satisfy needs of users. The use of the mmWave frequency signal spectrum offers a larger amount of bandwidth because these sections of the spectrum have not been used before for mobile communication. In order to practically implement the 5G mmWave network in the real-world scenario, the behavior of signal propagation among various channel conditions have been determined. Considering this, this paper discusses the results of outdoor measurement at 38 GHz for two different CI and Fl path loss models. The featured measurement outputs of LOS and NLOS for co- and cross-antenna polarizations were conducted at Universiti Teknologi Malaysia (UTM), Kuala Lumpur campus. Outcomes were gathered from simulation and real-world measurements to evaluate the system performance by representing several key factors, including cell-edge user throughput, average user throughput, fairness index, average cell throughput, and spectral efficiency for different numbers of users. The outcomes were examined at varied antenna configurations as well as at different channel bandwidths to proof the enhancement of overall network performance. For the CI model, the

LOS case measurement results for the PLE values were 3.0990 for V-V and 4.2556 for V-H configurations. Whereas, for the NLOS, the PLE values were 4.3202 and 4.214 for the V-V and V-H configurations, respectively. In the FI model, although it delivered significant results for the LOS case, its overall performance was poorer, as compared with the NLOS case for both V-V and V-H configurations. Moreover, the simulation results proved that the user throughputs for cross-polarization configuration decayed faster than the co-polarization for both the LOS and NLOS environments. However, the overall findings for the FI path loss model appeared to be lower than the CI path loss model, but the FI path loss model predicted a significant amount of performance that seemed suitable for some small cell LOS V-V scenarios. We believe that our findings presented in the paper are convenient and handy to test and implement the future generation 5G communication network for real-life environments. For future work, other potential 5G mmWave frequency spectra, such as 60 GHz and 70 GHz, will be studied. The spectra of such frequencies can utilize some of the optimal path loss propagation models, such as close-in with frequency weighted (CIF) and alpha-beta-gamma (ABG) models. We will investigate the influence of various beam-forming effects and will analyze their outcome on different massive MIMO conditions.

Data Availability: The data used to support the findings of this study are available from the corresponding authors upon request.

Author Contributions: F.Q. and M.N.H. conceived and designed the experiments; F.Q. and M.N.H. performed the experiments; F.Q., M.N.H. and K.D. analyzed the data; K.D., K.A.N., M.B.M., T.A.R., and I.S.A. contributed materials/reagents/analysis tools; F.Q. and M.N.H. wrote the paper.

Funding: The authors would like to acknowledge the University of Malaya (UM) grant: RK013-2018.

Acknowledgments: The authors would also like to thank the Universiti Teknologi Malaysia (UTM) Wireless Communication Centre (WCC) for their support.

Conflicts of Interest: The authors declare no conflict of interest.

References

1. Huang, S.; Cai, J.; Chen, H.; Zhang, H. Transmit power optimization for amplify-and-forward relay networks with reduced overheads. *IEEE Trans. Veh. Technol.* **2016**, *65*, 5033–5044. [CrossRef]
2. Liang, Q.; Durrani, T.S.; Liang, J.; Wang, X. Enabling Technologies for 5G Mobile Systems. *Mob. Inf. Syst.* **2016**, *2016*, 1945783. [CrossRef]
3. Hossain, E.; Hasan, M. 5G cellular: Key enabling technologies and research challenges. *IEEE Instrum. Meas. Mag.* **2015**, *18*, 11–21. [CrossRef]
4. Akyildiz, I.F.; Nie, S.; Lin, S.-C.; Chandrasekaran, M. 5G roadmap: 10 Key enabling technologies. *Comput. Netw.* **2016**, *106*, 17–48. [CrossRef]
5. Khawam, K.; Lahoud, S.; Ibrahim, M.; Yassin, M.; Martin, S.; El Helou, M.; Moety, F. Radio access technology selection in heterogeneous networks. *Phys. Commun.* **2016**, *18*, 125–139. [CrossRef]
6. Gachhadar, A.; Hindia, M.N.; Qamar, F.; Siddiqui, M.H.S.; Noordin, K.A.; Amiri, I.S. Modified genetic algorithm based power allocation scheme for amplify-and-forward cooperative relay network. *Comput. Electr. Eng.* **2018**, *69*, 628–641. [CrossRef]
7. Noordin, K.A.B.; Hindia, M.N.; Qamar, F.; Dimyati, K. Power Allocation Scheme Using PSO for Amplify and Forward Cooperative Relaying Network. In *Science and Information Conference*; Springer: Cham, Switzerland, 2018; Volume 857, pp. 636–647.
8. Rappaport, T.S.; Sun, S.; Mayzus, R.; Zhao, H.; Azar, Y.; Wang, K.; Wong, G.N.; Schulz, J.K.; Samimi, M.; Gutierrez, F. Millimeter wave mobile communications for 5G cellular: It will work! *IEEE Access* **2013**, *1*, 335–349. [CrossRef]
9. Rappaport, T.S.; Sun, S.; Shafi, M. 5G Channel model with improved accuracy and efficiency in mmWave bands. *IEEE 5G Tech. Focus* **2017**, *1*, 1–6.
10. Rappaport, T.S.; Sun, S.; Shafi, M. Investigation and comparison of 3GPP and NYUSIM channel models for 5G wireless communications. *arXiv* **2017**, arXiv:1707.00291.
11. Sun, S.; Rappaport, T.S.; Shafi, M. Hybrid beamforming for 5G millimeter-wave multi-cell networks. *arXiv* **2018**, arXiv:1803.03986.

12. Mogensen, P.; Pajukoski, K.; Tiirola, E.; Vihriala, J.; Lahetkangas, E.; Berardinelli, G.; Tavares, F.M.; Mahmood, N.H.; Lauridsen, M.; Catania, D.; et al. Centimeter-wave concept for 5G ultra-dense small cells. In Proceedings of the 2014 IEEE 79th Vehicular Technology Conference (VTC Spring), Seoul, South Korea, 18–21 May 2014; pp. 1–6.
13. Rappaport, T.S. 5G Millimeter Wave Wireless: Trials, Testimonies, and Target Rollouts. In Proceedings of the IEEE International Conference on Computer Communications, Honolulu, HI, USA, 15–19 April 2018.
14. Wang, T.; Li, G.; Huang, B.; Miao, Q.; Fang, J.; Li, P.; Tan, H.; Li, W.; Ding, J.; Li, J. Spectrum Analysis and Regulations for 5G. In *5G Mobile Communications*; Springer: Cham, Switzerland, 2017; pp. 27–50.
15. Udeshi, D.; Qamar, F. Quality Analysis of Epon Network for Uplink and Downlink Design. *Asian J. Eng. Sci. Technol.* **2014**, *4*, 78–83.
16. Hindia, M.N.; Qamar, F.; Rahman, T.A.; Amiri, I.S. A stochastic geometrical approach for full-duplex MIMO relaying model of high-density network. *Ad Hoc Netw.* **2018**, *74*, 34–46. [CrossRef]
17. Niu, Y.; Li, Y.; Jin, D.; Su, L.; Vasilakos, A.V. A survey of millimeter wave communications (mmWave) for 5G: Opportunities and challenges. *Wirel. Netw.* **2015**, *21*, 2657–2676. [CrossRef]
18. Panwar, N.; Sharma, S.; Singh, A.K. A survey on 5G: The next generation of mobile communication. *Phys. Commun.* **2016**, *18*, 64–84. [CrossRef]
19. Abbas, T.; Qamar, F.; Ahmed, I.; Dimyati, K.; Majed, M.B. Propagation channel characterization for 28 and 73 GHz millimeter-wave 5G frequency band. In Proceedings of the 2017 IEEE 15th Student Conference on Research and Development (SCOReD), Putrajaya, Malaysia, 13–14 December 2017; pp. 297–302.
20. Hong, W.; Baek, K.; Lee, Y. Quantitative analysis of the effects of polarization and pattern reconfiguration for mmWave 5G mobile antenna prototypes. In Proceedings of the 2017 IEEE Radio and Wireless Symposium (RWS), Phoenix, AZ, USA, 15–18 January 2017; pp. 68–71.
21. Hong, W. Solving the 5G Mobile Antenna Puzzle: Assessing Future Directions for the 5G Mobile Antenna Paradigm Shift. *IEEE Microw. Mag.* **2017**, *18*, 86–102. [CrossRef]
22. McClean, B. *Worldwide Cellphone Subscriptions Forecast to Exceed Worldwide Population in 2015*; IC Insights, INC.: Scottsdale, AZ, USA, 2014.
23. Qamar, F.; Dimyati, K.B.; Hindia, M.N.; Noordin, K.A.B.; Al-Samman, A.M. A Comprehensive Review on Coordinated Multi-Point Operation for LTE-A. *Comput. Netw.* **2017**, *123*, 19–37. [CrossRef]
24. Gupta, A.; Jha, R.K. A survey of 5G network: Architecture and emerging technologies. *IEEE Access* **2015**, *3*, 1206–1232. [CrossRef]
25. Andrews, J.G.; Buzzi, S.; Choi, W.; Hanly, S.V.; Lozano, A.; Soong, A.C.; Zhang, J.C. What will 5G be? *IEEE J. Sel. Areas Commun.* **2014**, *32*, 1065–1082. [CrossRef]
26. Gohil, A.; Modi, H.; Patel, S.K. 5G technology of mobile communication: A survey. In Proceedings of the 2013 International Conference on Intelligent Systems and Signal Processing (ISSP), Gujarat, India, 1–2 March 2013; pp. 288–292.
27. The Start of Something, 3rd Generation Partnership Project (3GPP). Phoenix, Arizona, USA, 19 September 2015. Available online: https://www.3gpp.org/news-events/1734-ran_5g (accessed on 1 April 2019).
28. Adler, R.F.; Charles, M. Preparing for a 5G World. The Aspen Institute: Washington, DC, USA, 2016; Available online: http://csreports.aspeninstitute.org/documents/PreparingFor5G.pdf (accessed on 1 April 2019).
29. Mittal, K.; Pathania, S.; Reddy, P.; Rawal, D. Channel State Information feedback overhead reduction using Arithmetic coding in massive MIMO systems. In Proceedings of the 2016 3rd International Conference on Signal Processing and Integrated Networks (SPIN), Noida, India, 11–12 February 2016; pp. 328–331.
30. Navabi, S.; Wang, C.; Bursalioglu, O.Y.; Papadopoulos, H. Predicting wireless channel features using neural networks. In Proceedings of the 2018 IEEE International Conference on Communications (ICC), Kansas City, MO, USA, 20–24 May 2018; pp. 1–6.
31. Chen, H.; Liu, L.; Matyjas, J.D.; Medley, M.J. Optimal resource allocation for sensing-based spectrum sharing D2D networks. *Comput. Electr. Eng.* **2015**, *44*, 107–121. [CrossRef]
32. Qamar, F.; Abbas, T.; Hindia, M.N.; Dimyati, K.B.; Noordin, K.A.B.; Ahmed, I. Characterization of MIMO propagation channel at 15 GHz for the 5G spectrum. In Proceedings of the 2017 IEEE 13th Malaysia International Conference on Communications (MICC), Johor Bahru, Malaysia, 28–30 November 2017; pp. 265–270.
33. Rappaport, T.S. *Wireless Communications: Principles and Practice*; Prentice Hall: Upper Saddle River, NJ, USA, 1996.

34. Qamar, F.; Siddiqui, M.H.S.; Dimyati, K.; Noordin, K.A.B.; Majed, M.B. Channel characterization of 28 and 38 GHz MM-wave frequency band spectrum for the future 5G network. In Proceedings of the 2017 IEEE 15th Student Conference on Research and Development (SCOReD), Putrajaya, Malaysia, 13–14 December 2017; pp. 291–296.
35. Ahamed, M.M.; Faruque, S. Propagation factors affecting the performance of 5G millimeter wave radio channel. In Proceedings of the 2016 IEEE International Conference on Electro Information Technology (EIT), Grand Forks, ND, USA, 19–21 May 2016; pp. 728–733.
36. Hindia, M.N.; Qamar, F.; Majed, M.B.; Rahman, T.A.; Amiri, I.S. Enabling remote-control for the power sub-stations over LTE-A networks. *Telecommun. Syst.* **2019**, *70*, 37–53. [CrossRef]
37. Rappaport, T.S.; MacCartney, G.R.; Samimi, M.K.; Sun, S. Wideband millimeter-wave propagation measurements and channel models for future wireless communication system design. *IEEE Trans. Commun.* **2015**, *63*, 3029–3056. [CrossRef]
38. Al-Samman, A.; Rahman, T.; Hindia, M.; Daho, A.; Hanafi, E.J.S. Path Loss Model for Outdoor Parking Environments at 28 GHz and 38 GHz for 5G Wireless. *Networks* **2018**, *10*, 672. [CrossRef]
39. Hossain, F.; Geok, T.K.; Rahman, T.A.; Hindia, M.N.; Dimyati, K.; Ahmed, S.; Tso, C.P.; Rahman, A.; Ziela, N. An Efficient 3-D Ray Tracing Method: Prediction of Indoor Radio Propagation at 28 GHz in 5G Network. *Electronics* **2019**, *8*, 286. [CrossRef]
40. Sun, S.; Rappaport, T.S.; Rangan, S.; Thomas, T.A.; Ghosh, A.; Kovacs, I.Z.; Rodriguez, I.; Koymen, O.; Partyka, A.; Jarvelainen, J. Propagation path loss models for 5G urban micro-and macro-cellular scenarios. In Proceedings of the 2016 IEEE 83rd Vehicular Technology Conference (VTC Spring), Nanjing, China, 15–18 May 2016; pp. 1–6.
41. Phillips, C.; Sicker, D.; Grunwald, D. A survey of wireless path loss prediction and coverage mapping methods. *IEEE Commun. Surv. Tutor.* **2013**, *15*, 255–270. [CrossRef]
42. Maccartney, G.R.; Rappaport, T.S.; Sun, S.; Deng, S. Indoor office wideband millimeter-wave propagation measurements and channel models at 28 and 73 GHz for ultra-dense 5G wireless networks. *IEEE Access* **2015**, *3*, 2388–2424. [CrossRef]
43. MacCartney, G.R.; Rappaport, T.S.; Samimi, M.K.; Sun, S. Millimeter-wave omnidirectional path loss data for small cell 5G channel modeling. *IEEE Access* **2015**, *3*, 1573–1580. [CrossRef]
44. Hur, S. Millimeter-wave channel modeling on 28 GHz. In Proceedings of the 9th IC1004 MC and Scientific Meeting, Ferrara, Italy, 5–7 February 2014. Available online: http://www.ic1004.org/index4f22.html?page=ferrara-italy---2014 (accessed on 1 April 2019).
45. Hur, S.; Cho, Y.J.; Kim, T.; Park, J. Millimeter-wave channel modeling based on measurements in in-building campus and urban environments at 28 GHz. In Proceedings of the 11th IC1004 MC and Scientific Meeting, Krakow, Poland, 24–26 September 2014. Available online: http://www.ic1004.org/indexb26f.html?page=krakow-poland---2014 (accessed on 1 April 2019).
46. Al-Samman, A.; Rahman, T.; Azmi, M.; Hindia, M.; Khan, I.; Hanafi, E. Statistical modelling and characterization of experimental mm-wave indoor channels for future 5G wireless communication networks. *PLoS ONE* **2016**, *11*, e0163034. [CrossRef]
47. Samimi, M.K.; Rappaport, T.S.; MacCartney, G.R. Probabilistic omnidirectional path loss models for millimeter-wave outdoor communications. *IEEE Wirel. Commun. Lett.* **2015**, *4*, 357–360. [CrossRef]
48. MacCartney, G.R.; Rappaport, T.S. 73 GHz millimeter wave propagation measurements for outdoor urban mobile and backhaul communications in New York City. In Proceedings of the 2014 IEEE International Conference on Communications (ICC), Sydney, NSW, Australia, 10–14 June 2014; pp. 4862–4867.
49. Rappaport, T.S.; Ben-Dor, E.; Murdock, J.N.; Qiao, Y. 38 GHz and 60 GHz angle-dependent propagation for cellular & peer-to-peer wireless communications. In Proceedings of the 2012 IEEE International Conference on Communications (ICC), Ottawa, ON, Canada, 10–15 June 2012; pp. 4568–4573.
50. Sulyman, A.I.; Nassar, A.T.; Samimi, M.K.; MacCartney, G.R.; Rappaport, T.S.; Alsanie, A. Radio propagation path loss models for 5G cellular networks in the 28 GHz and 38 GHz millimeter-wave bands. *IEEE Commun. Mag.* **2014**, *52*, 78–86. [CrossRef]
51. Zhong, Z.; Li, C.; Zhao, J.; Zhang, X. Height-dependent path loss model and large-scale characteristics analysis of 28 GHz and 38.6 GHz in urban micro scenarios. In Proceedings of the 2017 11th European Conference on Antennas and Propagation (EUCAP), Paris, France, 19–24 March 2017; pp. 1818–1822.

52. Al-Samman, A.; Hindia, M.; Rahman, T. Path loss model in outdoor environment at 32 GHz for 5G system. In Proceedings of the 2016 IEEE 3rd International Symposium on Telecommunication Technologies (ISTT), Kuala Lumpur, Malaysia, 28–30 November 2016; pp. 9–13.
53. Hur, S.; Cho, Y.J.; Kim, T.; Park, J.; Molisch, A.F.; Haneda, K.; Peter, M. Wideband spatial channel model in an urban cellular environments at 28 GHz. In Proceedings of the 2015 9th European Conference on Antennas and Propagation (EuCAP), Lisbon, Portugal, 13–17 April 2015; pp. 1–5.
54. Sayeed, A.; Brady, J.; Cheng, P.; Tayyab, U. Indoor channel measurements using a 28GHz multi-beam MIMO prototype. In Proceedings of the 2016 IEEE 84th Vehicular Technology Conference (VTC-Fall), Montreal, QC, Canada, 18–21 September 2016; pp. 1–5.
55. Larsson, C.; Olsson, B.-E.; Medbo, J. Angular Resolved Pathloss Measurements in Urban Macrocell Scenarios at 28 GHz. In Proceedings of the 2016 IEEE 84th Vehicular Technology Conference (VTC-Fall), Montreal, QC, Canada, 18–21 September 2016; pp. 1–5.
56. Huang, J.; Wang, C.-X.; Feng, R.; Sun, J.; Zhang, W.; Yang, Y. Multi-frequency mmWave massive MIMO channel measurements and characterization for 5G wireless communication systems. *IEEE J. Sel. Areas Commun.* **2017**, *35*, 1591–1605. [CrossRef]
57. Huang, J.; Feng, R.; Sun, J.; Wang, C.-X.; Zhang, W.; Yang, Y. Multi-frequency millimeter wave massive MIMO channel measurements and analysis. In Proceedings of the 2017 IEEE International Conference on Communications (ICC), Paris, France, 21–25 May 2017; pp. 1–6.
58. Sulyman, A.I.; Alwarafy, A.; MacCartney, G.R.; Rappaport, T.S.; Alsanie, A. Directional radio propagation path loss models for millimeter-wave wireless networks in the 28-, 60-, and 73-GHz bands. *IEEE Trans. Wirel. Commun.* **2016**, *15*, 6939–6947.
59. Park, J.-J.; Liang, J.; Lee, J.; Kwon, H.-K.; Kim, M.-D.; Park, B. Millimeter-wave channel model parameters for urban microcellular environment based on 28 and 38 GHz measurements. In Proceedings of the 2016 IEEE 27th Annual International Symposium on Personal, Indoor, and Mobile Radio Communications (PIMRC), Montreal, QC, Canada, 8–13 October 2017; pp. 1–5.
60. Chen, J.; Bin, F.; Ge, X.; Li, Q.; Wang, C.-X. A dual-directional path-loss model in 5G wireless fractal small cell networks. In Proceedings of the 2017 IEEE International Conference on Communications (ICC), Paris, France, 21–25 May 2017; pp. 1–6.
61. Sulyman, A.I.; Seleem, H.; Alwarafy, A.; Humadi, K.; Alsanie, A. Effects of Solar Radio Emissions on Outdoor Propagation Path Loss Models at 60 GHz bands for Access/backhaul links and D2D communications. *IEEE Trans. Antennas Propag.* **2017**, *65*, 6624–6635. [CrossRef]
62. Sasaki, M.; Nakamura, M.; Inomata, M.; Takatori, Y.; Kitao, K.; Imai, T. Path loss frequency dependence at 2–26 GHz in an urban macro cell environment. In Proceedings of the 2017 IEEE International Symposium on Antennas and Propagation and USNC/URSI National Radio Science Meeting, San Diego, CA, USA, 9–14 July 2017; pp. 601–602.
63. Karttunen, A.; Molisch, A.F.; Hur, S.; Park, J.; Zhang, C.J. Spatially Consistent Street-by-Street Path Loss Model for 28-GHz Channels in Micro Cell Urban Environments. *IEEE Trans. Wirel. Commun.* **2017**, *16*, 7538–7550. [CrossRef]
64. Hossain, F.; Geok, T.; Rahman, T.; Hindia, M.; Dimyati, K.; Abdaziz, A.J.S. Indoor Millimeter-Wave Propagation Prediction by Measurement and Ray Tracing Simulation at 38 GHz. *Symmetry* **2018**, *10*, 464. [CrossRef]
65. Hindia, M.N.; Al-Samman, A.M.; Rahman, T.A.; Yazdani, T. Outdoor large-scale path loss characterization in an urban environment at 26, 28, 36, and 38 GHz. *Phys. Commun.* **2018**, *27*, 150–160. [CrossRef]
66. Hindia, M.N.; Al-Samman, A.M.; Rahman, T.B.A. Investigation of large-scale propagation for outdoor-parking lot environment for 5G wireless communications. In Proceedings of the2016 IEEE 3rd International Symposium on Telecommunication Technologies (ISTT), Kuala Lumpur, Malaysia, 28–30 November 2016; pp. 14–18.
67. Sun, S.; MacCartney, G.R.; Rappaport, T.S. Millimeter-wave distance-dependent large-scale propagation measurements and path loss models for outdoor and indoor 5G systems. In Proceedings of the 2016 10th European Conference on Antennas and Propagation (EuCAP), Davos, Switzerland, 10–15 April 2016; pp. 1–5.
68. Sun, S.; Rappaport, T.S.; Thomas, T.A.; Ghosh, A.; Nguyen, H.C.; Kovács, I.Z.; Rodriguez, I.; Koymen, O.; Partyka, A. Investigation of prediction accuracy, sensitivity, and parameter stability of large-scale propagation path loss models for 5G wireless communications. *IEEE Trans. Veh. Technol.* **2016**, *65*, 2843–2860. [CrossRef]

69. Zheng, Y.; Blostein, S.D. Cooperative uplink cellular systems with multi-antenna relays and heterogeneous users. In Proceedings of the 2013 IEEE Global Communications Conference (GLOBECOM), Atlanta, GA, USA, 9–13 December 2013; pp. 3896–3901.
70. Sun, S.; Rappaport, T.; Shafi, M.; Tang, P.; Zhang, J.; Smith, P.J. Propagation models and performance evaluation for 5G millimeter-wave bands. *IEEE Trans. Veh. Technol.* **2018**, *67*, 8422–8439. [CrossRef]
71. MacCartney, G.R.; Zhang, J.; Nie, S.; Rappaport, T.S. Path loss models for 5G millimeter wave propagation channels in urban microcells. In Proceedings of the 2013 IEEE Global Communications Conference (GLOBECOM), Atlanta, GA, USA, 9–13 December 2013; pp. 3948–3953.
72. Evolved Universal Terrestrial Radio Access (E-UTRA); Radio Frequency (RF) system scenarios 'TR 36.942'. 3rd Generation Partnership Project (3GPP), Arizona, USA, January 2015. Available online: https://portal.3gpp.org/desktopmodules/Specifications/SpecificationDetails.aspx?specificationId=2592 (accessed on 1 April 2019).
73. Universal Mobile Telecommunications System (UMTS); RF System Scenarios; TR 25.942 version 14.0.0 Release 14. 3rd Generation Partnership Project (3GPP). Nice, France, April 2017. Available online: https://www.etsi.org/deliver/etsi_tr/125900_125999/125942/14.00.00_60/tr_125942v140000p.pdf (accessed on 1 April 2019).
74. Technical Specification Group RAN, E-UTRA; Physical Channels and Modulation TS 36.211'. 3rd Generation Partnership Project (3GPP). Arizona, USA, July 2012. Available online: https://portal.3gpp.org/desktopmodules/Specifications/SpecificationDetails.aspx?specificationId=2592 (accessed on 1 April 2019).
75. Arnau, J.; Atzeni, I.; Kountouris, M. Impact of LOS/NLOS propagation and path loss in ultra-dense cellular networks. In Proceedings of the 2016 IEEE International Conference on Communications (ICC), Kuala Lumpur, Malaysia, 22–27 May 2016; pp. 1–6.
76. Osseiran, A.; Monserrat, J.F.; Marsch, P. *5G Mobile and Wireless Communications Technology*; Cambridge University Press: Cambridge, UK, 2016.
77. Tsiropoulou, E.E.; Kastrinogiannis, T.; Papavassiliou, S. Uplink power control in qos-aware multi-service cdma wireless networks. *J. Commun.* **2009**, *4*, 654–668. [CrossRef]
78. Kastrinogiannis, T.; Tsiropoulou, E.-E.; Papavassiliou, S. Utility-based uplink power control in CDMA wireless networks with real-time services. In *Proceedings of the International Conference on Ad-Hoc Networks and Wireless*; Springer: Berlin, German, 2008; pp. 307–320.
79. Lee, P.; Lee, T.; Jeong, J.; Shin, J. Interference management in LTE femtocell systems using fractional frequency reuse. In Proceedings of the 2010 the 12th International Conference on Advanced Communication Technology (ICACT), Phoenix Park, South Korea, 7–10 February 2010; Volume 2, pp. 1047–1051.
80. Muhammad, S.S.; Kohldorfer, P.; Leitgeb, E. Channel modeling for terrestrial free space optical links. In Proceedings of the 2005 7th International Conference Transparent Optical Networks, Barcelona, Catalonia, Spain, 7 July 2005; Volume 1, pp. 407–410.
81. Qamar, F.; Hindia, M.N.; Abbas, T.; Dimyati, K.B.; Amiri, I.S. Investigation of QoS Performance Evaluation over 5G Network for Indoor Environment at millimeter wave Bands. *Int. J. Electron. Telecommun.* **2019**, *65*, 95–101.
82. Chayon, H.R.; Dimyati, K.; Ramiah, H.; Reza, A.W. An Improved Radio Resource Management with Carrier Aggregation in LTE Advanced. *Appl. Sci.* **2017**, *7*, 394. [CrossRef]
83. Kim, H.; Kim, K.; Han, Y.; Yun, S. A proportional fair scheduling for multicarrier transmission systems. In Proceedings of the 2004 IEEE 60th Vehicular Technology Conference (VTC2004-Fall), Los Angeles, CA, USA, 26–29 September 2004; Volume 1, pp. 409–413.
84. Djouama, A.; Lim, M.-S. Reduction of the feedback delay effect on a proportional fair scheduler in LTE downlink using nonlinear support vector machine prediction. *AEU Int. J. Electron. Commun.* **2015**, *69*, 1393–1402. [CrossRef]
85. Ge, X.; Cheng, H.; Guizani, M.; Han, T. 5G wireless backhaul networks: Challenges and research advances. *IEEE Netw.* **2014**, *28*, 6–11. [CrossRef]

86. Marinello, J.C.; Abrão, T. Pilot distribution optimization in multi-cellular large scale MIMO systems. *AEU Int. J. Electron. Commun.* **2016**, *70*, 1094–1103. [CrossRef]
87. Jungnickel, V.; Manolakis, K.; Zirwas, W.; Panzner, B.; Braun, V.; Lossow, M.; Sternad, M.; Apelfrojd, R.; Svensson, T. The role of small cells, coordinated multipoint, and massive MIMO in 5G. *IEEE Commun. Mag.* **2014**, *52*, 44–51. [CrossRef]